

# Decoupling of paramagnetic and ferrimagnetic AMS development during the experimental chemical compaction of illite shale powder

Rolf H.C. Bruijn,<sup>1,\*</sup> Bjarne S.G. Almqvist,<sup>1</sup> Ann M. Hirt<sup>2</sup> and Philip M. Benson<sup>3</sup>

<sup>1</sup>Geological Institute, ETH Zurich, Sonneggstrasse 5, CH-8092 Zurich, Switzerland. E-mail: bruijn@levee.wustl.edu

<sup>2</sup>Geophysical Institute, ETH Zurich, Sonneggstrasse 5, CH-8092 Zurich, Switzerland

<sup>3</sup>School of Earth & Environmental Sciences, University of Portsmouth, Burnaby Building, Burnaby Road, PO1 3QL Portsmouth, UK

Accepted 2012 November 23. Received 2012 November 21; in original form 2012 January 8

## SUMMARY

Inclination shallowing of detrital remanent magnetization in sedimentary strata has solely been constrained for the mechanical processes associated with mud deposition and shallow compaction of clay-rich sediment, even though a significant part of mud diagenesis involves chemical compaction. Here we report, for the first time, on the laboratory simulation of magnetic assemblage development in a chemically compacting illite shale powder of natural origin. The experimental procedure comprised three compaction stages that, when combined, simulate the diagenesis and low-grade metamorphism of illite mud. First, the full extent of load-sensitive mechanical compaction is simulated by room temperature dry axial compression. Subsequently, temperature controlled chemical compaction is initiated by exposing the sample in two stages to amphibolite or granulite facies conditions (temperature is 490 to 750°C and confining pressure is 170 or 300 MPa) both in the absence (confining pressure only) and presence of a deformation stress field (axial compression or confined torsion). Thermodynamic equilibrium in the last two compaction stages was not reached, but illite and mica dehydroxylation initiated, thus providing a wet environment. Magnetic properties were characterized by magnetic susceptibility and its anisotropy (AMS) in both high- and low-applied field. Acquisition of isothermal remanent magnetization (IRM), stepwise three-component thermal de-magnetization of IRM and first-order reversal curves were used to characterize the remanence-bearing minerals. During the chemical compaction experiments ferrimagnetic iron-sulphides formed after reduction of magnetite and detrital pyrite in a low sulphur fugacity environment. The degree of low-field AMS is unaffected by porosity reduction from 15 to ~1 per cent, regardless of operating conditions and compaction history. High-field paramagnetic AMS increases with compaction for all employed stress regimes and conditions, and is attributed to illite transformation to iron-bearing mica. AMS of authigenic iron-sulphide minerals remained constant during compaction indicating an independence of ferrimagnetic fabric development to chemical compaction in illite shale powder. The decoupling of paramagnetic and ferrimagnetic AMS development during chemical compaction of pelite contrasts with findings from mechanical compaction studies.

**Key words:** Magnetic fabrics and anisotropy; Magnetic mineralogy and petrology; Rock and mineral magnetism.

## 1 INTRODUCTION

Mud redeposition and clay-rich sediment compaction experiments have greatly improved our understanding of inclination shallowing of detrital remanent magnetization recorded in marine sedimentary sections (Blow & Hamilton 1978; Anson & Kodama 1987; Deamer & Kodama 1990; Jackson *et al.* 1991; Sun & Kodama 1992). Based

on these shallow basin simulation studies several mechanisms that couple remanence bearing minerals to clay particles or clay particle aggregates have been proposed: (1) electrostatic forces that cause positively charged ferrimagnetic minerals to adhere to the surface of negatively charged clay particles (Anson & Kodama 1987), (2) bonding of ferrimagnetic minerals and clay particles by Van der Waals forces (Deamer & Kodama 1990; Lu *et al.* 1990; Katari & Tauxe 2000) and (3) incorporation of remanence bearing particles into clay domains, that is aggregation of clay particles (Deamer & Kodama 1990). Regardless of the importance of specific mechanisms involved in particle rotation and alignment in response to the

\* Corresponding address: Washington University in St. Louis (Earth and Planetary Sciences) Campus box 1169, One Brookings Drive St. Louis, MO 63130 United States

increasing overburden load, the axis of easiest magnetization rotates towards a shallower orientation (Anson & Kodama 1987; Arason & Levi 1990a; Deamer & Kodama 1990; Sun & Kodama 1992). In addition, below loads of 0.02 MPa, inclination may also shallow as a result of preferred disturbance of unattached (free) subvertical ferrimagnetic minerals (Sun & Kodama 1992).

The work of Blow & Hamilton (1978), Anson & Kodama (1987), Deamer & Kodama (1990) and Sun & Kodama (1992) provided great insight into the effect of mud deposition and subsequent compaction on inclination shallowing, demonstrating activated fluid expulsion, grain close packing and grain rotation/reorientation in their mud samples even at the relatively low maximum load (<2.5 MPa) and room temperature conditions. Compaction (i.e. the reduction of pore volume or porosity) because of these processes is typically referred to as mechanical compaction and is restricted to the upper ~2 km of buried strata in sedimentary basins (e.g. Rieke & Chilingarian 1974; Bjørlykke 1998). In deeper domains, diagenesis continues at higher temperature activating mineral transformation; most importantly first smectite to illite (~70 to 150°C) and later (250 to 350°C) illite to phengite (e.g. Hower *et al.* 1976; Merriman & Peacor 1999). Silica release associated with these transformation reactions is a primary source for cementation (e.g. Towe 1962; Boles & Franks 1979; Land *et al.* 1997; Van de Kamp 2008; Day-Stirrat *et al.* 2010). Porosity reduction associated with cementation and mineral transformation is generally referred to as chemical compaction (e.g. Bjørlykke 1998). The full extent of mud diagenesis or lithification includes both mechanical and chemical compaction.

Outside the domain of rock magnetism, mechanical compaction of mud has been extensively studied in the laboratory, using modified oedometric cells that impose a uniaxial stress field of up to 100 MPa effective normal stress (simulating burial to 6.5–7.0 km) and temperature (<150°C) on a dry or fluid-saturated sample (e.g. Vasseur *et al.* 1995; Nygård *et al.* 2004; Mondol *et al.* 2007; Voltolini *et al.* 2009; Fawad *et al.* 2010; Schneider *et al.* 2011). The experiments show good agreement with porosity-depth trends derived from well logs and drill cores until the onset of chemical compaction marked by the first occurrence of authigenic illite (Mondol *et al.* 2007; Peltonen *et al.* 2009). Despite the notable effect of chemical compaction on mudstone and shale petrophysical properties, laboratory studies that support the observations from nature are lacking. Heating and stress field limitations of the customized oedometric cells, and the slow kinetics of clay transformation reactions limited research in this direction (Bjørlykke 1998).

Recently, an exploratory study by Bruijn (2012) demonstrated that mud diagenesis and very low-grade metamorphism can be simulated in a laboratory environment, provided underlying mineral transformation and cementation processes are accelerated to complete within laboratory timescales. By using rock deformation apparatus instead of modified oedometric cells, and geologically extraordinary temperature (ambient temperature and 490–750°C) and pressure (160 and 300 MPa) conditions, powder of illite shale could be compacted down to ~1 per cent in a compaction procedure that simulates the transformation of illite mud into lower greenschist facies metapelite. Thermodynamic forward modelling revealed that the mineral reactions involving phyllosilicate minerals are barely sensitive to pressure and that in chemical equilibrium high-grade amphibolite and granulite facies mineral assemblages can be expected. The duration of the experiments was however too short for equilibrium to be reached, keeping the metamorphic grade low (Bruijn 2012).

Here we report on the evolution of magnetic properties in experimentally compacted illite shale powder (origin Maplewood Shale,

USA) from the study of Bruijn (2012). The range in porosity (1 to 15 per cent) and the mechanism behind compaction differ significantly from those investigated in laboratory studies that looked at inclination shallowing in the realm of mechanical compaction (Blow & Hamilton 1978; Anson & Kodama 1987; Deamer & Kodama 1990; Jackson *et al.* 1991; Sun & Kodama 1992). Samples are characterized by their bulk magnetic susceptibility ( $K_m$ ), and anisotropy of magnetic susceptibility (AMS) in both low- and high fields. In addition, magnetic remanence is described using acquisition of isothermal remanent magnetization (IRM), stepwise thermal demagnetization of a three-component IRM (Lowrie 1990), and construction of first-order reversal curves (FORC) diagrams (Pike *et al.* 1999; Roberts *et al.* 2000). We place particular emphasis upon defining subfabrics of the paramagnetic (phyllosilicates) and ferrimagnetic phases and their evolution with compaction, to investigate for the first time inclination shallowing in the realm of chemical compaction.

## 2 METHOD

### 2.1 Source material

The material used in the exploratory chemical compaction experiments of Bruijn (2012) is the illite-rich Maplewood Shale from the Lower Clinton Group (Llandoveryan) in the Appalachian basin of Western New York (e.g. Brett *et al.* 1990; Rogers *et al.* 1990), supplied by Ward's Natural Science®. The mineral composition of Maplewood Shale consists of illite, clinocllore, quartz, and phengite as primary phases (>5 vol. per cent) with smectite, pyrite, rutile, apatite and biotite as secondary phases (<5 vol. per cent), as determined by scanning electron microscopy (SEM) and X-ray diffraction (XRD; Figs 1a and b). Similar findings have been reported by Saffer & Marone (2003) and Kaszuba *et al.* (2005). Based on 5.0 km burial depth estimates for nearby Late-Ordovician Trenton Group carbonates (Friedman 1987) Maplewood Shale is inferred to have experienced typical smectite illitization under late

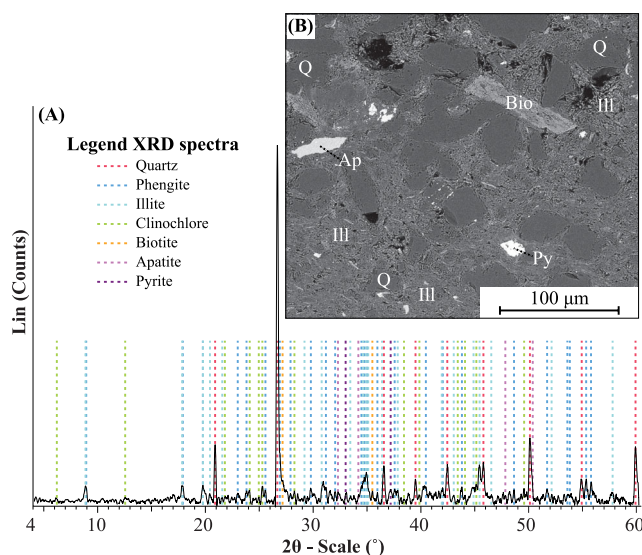


**Figure 1.** (a) X-ray powder diffraction spectrum for natural Maplewood Shale (NAT), with mineral identification for the major peaks. (b) SEM backscatter electron micrograph of Maplewood Shale, with mineral phase identification using atomic number contrast, grain shape, and energy dispersive spectroscopy. Mineral abbreviations are Q, quartz; Ill, illite; Bio, biotite; Py, pyrite; Ap, apatite.

**Table 1.** Compaction history and statistical data for bulk magnetic susceptibility of natural Maplewood Shale and derived experimentally compacted synthetic metapelites.

Sample group	Compaction history	Mean $K_m$ ( $\mu$ SI)	Min $K_m$ ( $\mu$ SI)	Max $K_m$ ( $\mu$ SI)	$N^a$	Standard error <sup>b</sup>
Maplewood Shale						
NAT	Nature	223	200	266	11	7.5
NAT (Pwd) <sup>c</sup>	Nature	2516	1341	3938	13	323.4
Synthetic metapelites						
HIP1	1 + 2	497	473	547	10	7.6
HIP2	1 + 2 + 3a	967	559	1122	10	70.2
PAT1 (C) <sup>d</sup>	1 + 2 + 3b	421	209	709	21	31.2
PAT1 (P <sub>c</sub> ) <sup>e</sup>	1 + 2 + 3b	367	234	469	4	58.6
PAT1 (C <sub>750</sub> ) <sup>f</sup>	1 + 2 + 3b	455	442	469	2	13.5
PAT1 (C <sub>p</sub> ) <sup>g</sup>	1 + 2 + 3b	333	255	408	5	24.2
PAT1 (T) <sup>h</sup>	1 + 2 + 3b	846	262	1430	2	584.1

<sup>a</sup> $n$  = number of measurements.

<sup>b</sup>Standard error =  $(\sigma n^{-1})^{0.5}$ , where  $\sigma$  is standard deviation.

<sup>c</sup>(Pwd) refers to crushed shale (i.e. illite shale powder before compaction stage 1).

<sup>d</sup>(C) refers to axial compression conditions during compaction stage 3b.

<sup>e</sup>(P<sub>c</sub>) refers to confining pressure conditions during compaction stage 3b.

<sup>f</sup>(C<sub>750</sub>) refers to axial compression at 750°C conditions during compaction stage 3b.

<sup>g</sup>(C<sub>p</sub>) refers to axial compression and pore pressure conditions during compaction stage 3b.

<sup>h</sup>(T) refers to confined torsion conditions during compaction stage 3b.

diagenetic to anchizone burial conditions, which led to chemical compaction already under natural circumstances (e.g. Hower *et al.* 1976; Merriman & Peacor 1999). Consequently, the experimental chemical compaction of illite shale powder relied on illite/phengite transformation, which is naturally activated under epizone conditions (e.g. Merriman & Peacor 1999; Van de Kamp 2008). Other illite-rich shales proved unsuitable because they were either contaminated with other clay minerals and/or carbonates, which would unnecessarily complicate the chemistry of the system or comprised uncharacteristic average grain size because of a large fraction of silt- and sand-size detrital grains; not representing the classic view of clay-dominated shale.

Illite shale powder [hereafter referred to as NAT (Pwd)] was produced by crushing fragments of Maplewood Shale (NAT) using a high power tungsten ‘shaker’. NAT (Pwd) has 15 vol. per cent clay (<2  $\mu$ m), 80 vol. per cent silt (2–63  $\mu$ m) and 5 vol. per cent sand (>63  $\mu$ m) by size fraction, and an average grain size of 20  $\mu$ m, as determined by laser diffraction using a Malvern Mastersizer 2000 with ultrasonic agitation.

## 2.2 Experimental background

To achieve chemical compaction of illite shale powder in laboratory timescales, Bruijn (2012) developed a three-stage compaction procedure that made use of three different rock deformation apparatus and three distinct stress fields. The sequence of experiments involves load-sensitive mechanical compaction, followed by temperature-sensitive chemical compaction with the absence or presence of directed constant strain-rate deformation, thus essentially simulating diagenesis and very low-grade metamorphism of illite mud with and without tectonic forces. Besides addressing chemical compaction for the first time experimentally, by applying and withholding simulated tectonic forces, this novel procedure also allowed the evaluation of the role of the stress field on the porosity, microstructural, chemical and magnetic development of illite mud diagenesis and low-grade metamorphism. The role of the stress field is evaluated by comparing AMS development during compaction under lithostatic (i.e. pressure and temperature) conditions with its

development during compaction under non-lithostatic or dynamic (i.e. pressure, temperature and strain rate or stress) conditions.

To highlight the changes in mineral composition with respect to the illite shale starting material the lithified and metamorphosed low-porosity samples in Bruijn (2012) are referred to in this paper as synthetic metapelites. For interpretation purposes, the synthetic metapelites are grouped according to their compaction stage history rather than treated individually (Table 1).

### 2.2.1 Compaction stage 1

In stage 1, crushed illite shale [NAT (Pwd)] was compressed inside stainless steel canisters enclosed within a heavy steel casing using a ram to provide ~200 MPa of vertical stress ( $\sigma_v$ ) (Fig. 2a). The employed stress field is known as confined or axial compression and is categorized as non-lithostatic. Axial or confined compression is the stress field state in which one principal stress is greater than the other two that are equal and greater than zero (Fig. 2d). In rock deformation experiments such a stress field is established when a (pressurized) confining medium imposes a horizontal force, and a vertical actuator-driven ram or piston imposes an additional force on a sample. Axial compression typically results in vertical shortening of the sample, which in the case of pure shear deformation (no volume loss) is compensated for by horizontal extension or in the case of compaction is accommodated purely by volume reduction of pore space. In compaction stage 1, a hydraulic ram provided the maximum stress ( $\sigma_v$ ), whereas in the horizontal plane the steel casing provided the minimum stress ( $\sigma_h$ ; Fig. 2d).

The excessive load (>100 MPa) ensured exhaustion of mechanical compaction processes and allowed the inference that compaction in later stages could be solely ascribed to chemical processes (e.g. Rieke & Chilingarian 1974; Vasseur *et al.* 1995; Nygård *et al.* 2004; Mondol *et al.* 2007). Stage 1 simulated cold sediment burial to a depth of 11–13 km, using a modified Pascal’s law with an average effective density of water-saturated sedimentary rock of 1.5 kg m<sup>-3</sup>, but without the application of heat, and solely initiated mechanical compaction; that is no lithification or mineral alteration of the illite shale powder.

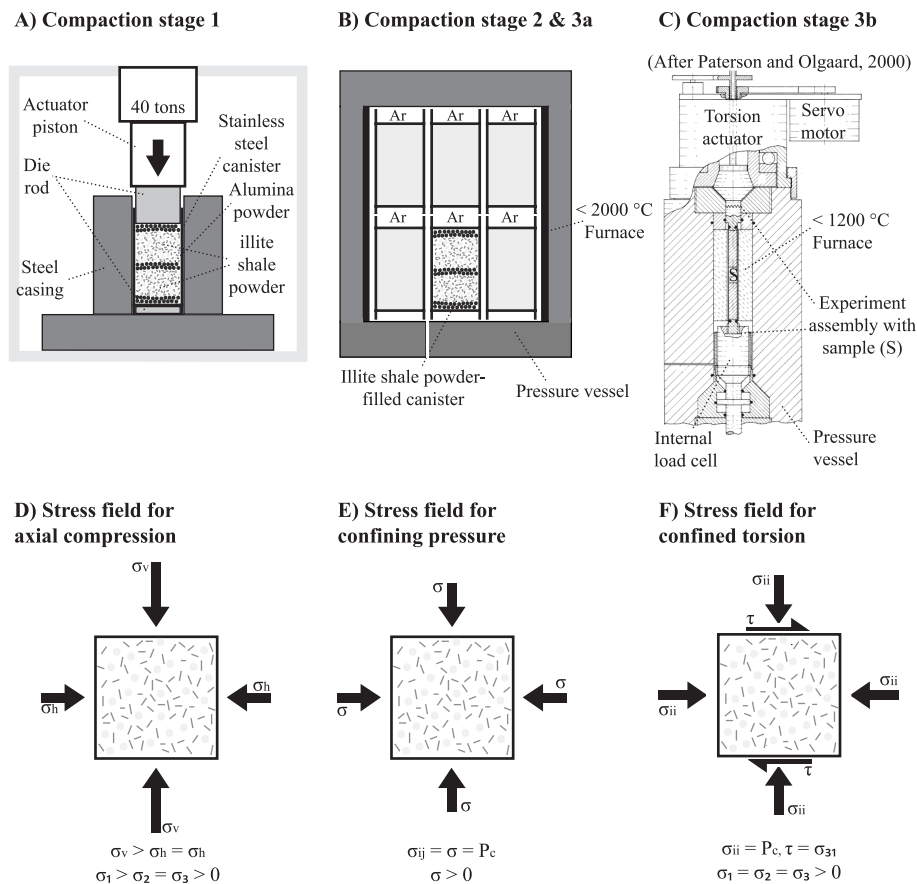


**Figure 2.** (a–c) Schematic, but unscaled drawings of the compaction apparatus used in the experimental compaction procedure in Bruijn (2012). (a) A 40 tons hydraulic press in combination with a stainless steel canister and heavy steel casing, used for compaction stage 1 experiments. (b) The hot isostatic press (HIP) apparatus used for compaction stages 2 and 3a experiments. Together with other canisters, the mechanically compacted illite shale powder is heat treated under a confining pressure stress field. (c) The Paterson-type HPT gas-medium testing machine (Paterson apparatus) equipped with axial and torsion actuators used for compaction stage 3b experiments. (d–f) 2-D representations of the stress fields associated with (d) axial compression, (e) confining pressure and (f) confined torsion, used in Bruijn (2012) to simulate chemical compaction of illite shale. Axial compression and confined torsion are considered non-lithostatic stress fields. Confining pressure is the laboratory equivalent of a lithostatic stress field.

### 2.2.2 Compaction stage 2 and 3a

In stage 2, illite shale powders were thermally further compacted for 24 hrs inside the canisters from stage 1 by pressurized and heated argon gas (170 MPa and 590°C), using a hot isostatic press (HIP) apparatus (Fig. 2b). The compressed gas exerts an equal force to the canisters from all directions (Fig. 2e), creating a stress field commonly referred to as confining pressure. Compaction by confining pressure is the laboratory equivalent of lithostatic pressure in nature. A confining pressure stress field theoretically results in pure contraction (i.e. volume loss by equal shortening in all directions). In practice, however, shortening often differs, with maximum strain in the vertical orientation.

Unlike other studies that have used a HIP for material compaction (e.g. Till *et al.* 2010), oxygen fugacity during stage 2 was not buffered. Stage 2 lithified the illite shale powder and initiated the transformation of illite into phengite, thereby creating a moderately porous (porosity 11–15 per cent) synthetic metapelite. The resulting canisters were then split into two groups. The first of which was further compacted in the HIP (170 MPa and 490°C), which is denoted compaction stage 3a. From the second group cylindrical samples were prepared for stage 3b, by drilling with a hollow diamond coring drill-bit to yield samples of 10 or 15 mm diameter and of 5–20 mm length via wet abrasive paper polishing. Stages 2 and

3a simulated very low to low-grade metamorphism pelite transformation under lithostatic conditions, by exposing illite shale powder for a relative short period to amphibolite facies conditions.

### 2.2.3 Compaction stage 3b

In stage 3b, compaction was continued using a Paterson-type HPT gas-medium testing machine (Paterson apparatus) equipped with axial and torsion actuators and pore-pressure system (Fig. 2c; Paterson 1990; Paterson & Olgaard 2000). Constant argon gas pressure of 300 MPa was typically applied to pressurize the sample assembly inside the pressure vessel, whereas the internal furnace provided a fixed temperature of 500, 650, 700 or 750°C. Compaction in stage 3b tests was enforced by exposing the sample to heat and either (1) a confining pressure or (2) an axial compression or (3) a confined torsion stress field (Figs 2d and f), which led to predominantly contraction, pure or, simple shear deformation of the sample, respectively. Confined torsion is an adaptation of axial compression in that, instead of an additional vertical force, a torque is enforced on the sample by means of a servo-motor-controlled rotational twist (Fig. 2f; Paterson & Olgaard 2000). All principal stresses are equal, but a shear stress in the horizontal plane is nonzero. Consequently, a vertical line in a twisting sample deforms by simple shear. Confined torsion is a non-lithostatic type of stress field.

Activation of an externally mounted torsion or axial actuator imposed constant twist rates (torsion) or displacement rates (axial compression) and resulted in shear- and axial- strain rates, respectively, ranging from  $10^{-6}$  to  $10^{-4}$  s $^{-1}$ . In the case of axial compression, maximum sample shortening was 20 per cent. Although, simple shear deformation (torsion) was limited to a shear strain of 0.3. To study the sensitivity of chemical compaction to (effective) pressure and the addition of pore pressure, Bruijn (2012) also performed single axial compression tests at 500, 650 and 700°C with additional argon gas pressure inside the sample (20 or 50 MPa), using the pore pressure system available for a Paterson apparatus. Stage 3b simulated very low to low-grade metamorphism illite mud transformation under non-lithostatic conditions by reheating illite shale powder for a relative short period to amphibolite or granulite facies conditions whereas forcing deformation in a pure shear or simple shear deformation style.

#### 2.2.4 Rationale experiment conditions

Relying on the fact that mineral transformation rates increase with temperature, unrealistically high temperature (amphibolite to granulite facies) and strain rate conditions for deep sedimentary basins and low-grade metamorphic terranes where chemical compaction is typically observed were applied to accomplish low-porosity (<15 per cent) compaction. Experiment conditions correspond to crustal geothermal gradients varying between roughly 40 and 85°C km $^{-1}$ . These extraordinary geothermal gradients are not only because of machine limitations, which capped pressure to 300 MPa, but are also necessary to witness illite transformation into phengite and associated silica cementation within laboratory timescales. As concomitant mineral reactions driving towards an amphibolite or granulite facies mineral assemblage are barely accelerated by the applied temperature and pressure conditions during stages 2 and 3, they could be considered of negligible importance (Bruijn 2012). The applied strain rates allow reaching engineering strain values theoretically needed for complete compaction ( $\epsilon > 15$  per cent) within hours rather than geological time (for  $d\epsilon/dt = 10^{-13}$  s $^{-1}$ ). The use of extraordinary experimental parameters is typically justified when petrophysical properties of experimentally deformed samples corresponds with those for equivalent natural samples. In this study, intact Maplewood Shale provides comparison material.

By using illite-rich shale as starting material for the compaction experiments the low temperature chemical compaction inducing mineral transformation in mud (i.e. smectite to illite) during diagenesis has not been simulated. The reason for using illite-rich shale and therefore placing the focus solely on the illite to phengite transformation reaction is that smectite illitization can only be accelerated to 200°C before phengite forms at the expense of illite (Merriman & Frey 1999; Merriman & Peacor 1999), whereas phengite does not decompose until a temperature of 610–650°C at 170–300 MPa (Bruijn 2012). The temperature range for the acceleration of the illite to phengite transformation is much wider than that for the smectite to illite transformation, which means that the likelihood of completing the former reaction within laboratory timescales is greatest. Using a smectite-rich mud as starting material would have two major disadvantages: (1) it would have activated multiple chemical compaction inducing reactions, and complicate the interpretation of resulting synthetic metapelites, or (2) it would not complete illitization of the smectite within the duration of an experiment because of restricted temperature conditions.

### 2.3 Sample analysis

The degree of compaction was quantified by porosity, measured with a Micromeritics AccuPyc 1330 helium pycnometer. To ensure accuracy the calculations were based on an average of seven volume determinations of cylindrical samples (Bruijn 2012).

Bulk magnetic susceptibility was determined with a low-field Agico KLY-2 susceptibility bridge (300 Am $^{-1}$  applied field at 875 Hz frequency). Dimensionless susceptibility measurements were normalized by grain volume to yield units SI. Degree of low-field AMS is expressed by  $P_j$  (Jelinek 1981, eq. 4), which is a measure of the scatter of the natural logarithms of the eigen values ( $k_1 \geq k_2 \geq k_3$ ) of the symmetric second rank magnetic susceptibility tensor.  $P_j$  is favoured over the anisotropy degree  $P = k_1/k_3$  to account for principal susceptibilities ratios rather than differences and to include the intermediate susceptibility ( $k_2$ ) (Jelinek 1981). High-field AMS, expressed by  $\Delta k$  (i.e.  $k_1 - k_3$ ), was measured using a torque magnetometer (Bergmüller *et al.* 1994), and magnetic subfabrics were isolated following the method proposed by Martín-Hernández & Hirt (2001). Sample torque was measured over 360° in 30° steps about three orthogonal axes, for six fields ranging between 0.5 and 1.5 T, as well as in the absence of an applied field. High-field AMS measurements permit the separation of ferrimagnetic AMS from paramagnetic and diamagnetic AMS (Martín-Hernández & Hirt 2001). IRM and FORC data were acquired to characterize the ferrimagnetic mineral phases present during various stages of the compaction procedure. IRM acquisition was imparted with a Princeton Measurements Corporation vibrating sample magnetometer (VSM; Model 3900). The FORC measurements used a saturating field of 1.0 T, with 100 ms averaging time and 130 reversal curves. A FORC diagram is a contour plot of the FORC distribution with coercive force ( $H_c$ ) on the horizontal axis and interaction field ( $H_u$ ) on the vertical axis (e.g. Pike *et al.* 1999). In addition, the orthogonal three-component IRM (Lowrie 1990) was produced with an ASC Model IM-10–30 impulse magnetizer. The cross-components were applied to a HIP1 and HIP2 sample in three orthogonal directions; a different field magnitude was applied along each individual direction. The magnitude of the fields was 1000 mT, 500 mT, and 200 mT. After application the three-component IRM was thermally demagnetized to a maximum temperature of 600°C.

### 3 RESULTS

The three-stage compaction of illite shale powder resulted in synthetic metapelites with a porosity range from 16 to 1 per cent. Porosity for natural Maplewood Shale (NAT) has been determined at  $2.7 \pm 0.2$  per cent (Bruijn 2012). The mean  $K_m$  of NAT samples increases by one order of magnitude subsequent to crushing [NAT (Pwd)]; however, variation exists among batches of the powder (Table 1). The highest susceptibility is recorded in illite shale powder that was compacted into HIP2 synthetic metapelites. During compaction stage 2 and 3a, susceptibility decreased. PAT1 samples yielded smaller values for  $K_m$  in comparison with HIP1 samples.

The IRM for powdered Maplewood Shale [NAT (Pwd)] closely resembles the typical behaviour of magnetite/maghemite, with saturation above an applied field of 0.3 T (Fig. 3). Distinction between magnetite and maghemite is irrelevant for the purpose of this study as AMS in both minerals is controlled by grain shape (Dunlop & Özdemir 1997). The synthetic metapelites of HIP1, HIP2 and PAT1 (C) sample groups, however, have different IRM acquisition with an unsaturated component. Minimal variation in IRM acquisition is observed among the synthetic metapelites (Fig. 3).

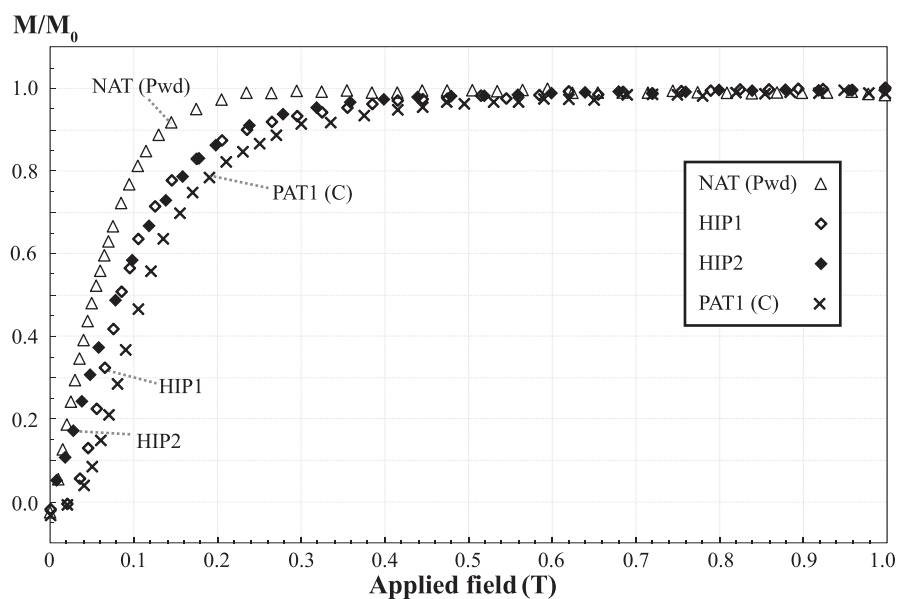


**Figure 3.** Isothermal remanence magnetization (IRM) acquisition curves for samples of crushed Maplewood Shale [NAT (Pwd)], and synthetic metapelites [HIP1, HIP2 and PAT1 (C)].  $M_0$  is the value for  $M$  at an applied field of 1.0 T.

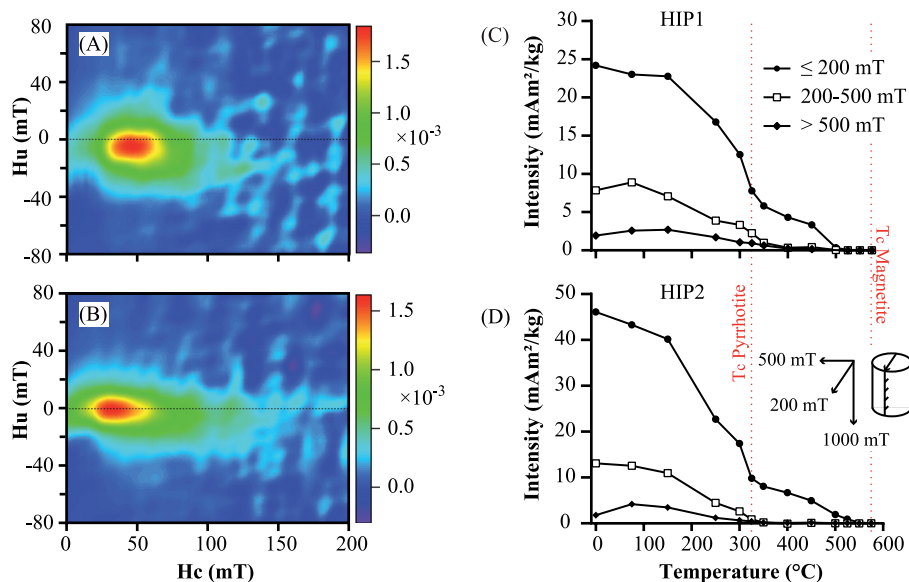


**Figure 4.** (a–b) First-order reversal curves (FORC) diagrams computed with FORCinel v.1.17 (Harrison & Feinberg 2008) obtained from a HIP1, HIP2 and PAT1 (c) sample showing (a) FORC distribution type 1 and (b) FORC distribution type 2. (c–d) Stepwise thermal demagnetization of acquired IRM curves obtained from (c) a HIP1 sample with a type 1 FORC distribution and (d) a HIP2 sample with a type 2 FORC distribution. For reference the Curie temperature ( $T_c$ ) of pyrrhotite (325°C) and magnetite (575°C) are marked.

Two distinct FORC distribution types emerged from the analysis of HIP1, PAT1 (C) and HIP2 samples (Figs 4a and b). Type 1 shows a broad coercivity distribution between 20 and 90 mT with a maximum between 40 to 55 mT, and a distribution in interaction fields that centres around  $-6$  mT (Fig. 4a). This FORC distribution is typical for iron sulphides, such as greigite ( $\text{Fe}_7\text{S}_4$ ; Roberts *et al.* 2006, 2011). Type 2 also shows a broad coercivity distribution up to 150 mT, with a peak distribution between 25 and 35 mT. The distribution in interaction fields is narrower and centred around  $H_c = 0$  (Fig. 4b). This FORC distribution is more difficult to ascribe simply to a single phase. The tail in the distribution suggests the presence of a higher coercivity phase, such as pyrrhotite ( $\text{Fe}_7\text{S}_8$ ) or possibly hematite ( $\alpha\text{-Fe}_2\text{O}_3$ ; Roberts *et al.* 2006). Demagnetization of the three-component IRM shows that the bulk of the magnetic

remanence for both HIP1 and HIP2 is carried by a low coercivity phase ( $< 200$  mT; Figs 4c and d). The low coercivity component, and to some extent the intermediate coercivity component, display a marked decrease in remanence between 320 and 350°C. The remanence is completely removed by 525–550°C, which is observed only in the low coercivity component. The large decrease seen around 320–350°C is indicative for the demagnetization (unblocking) of pyrrhotite or alternatively, the breakdown of greigite. The higher temperature remanence unblocking, between 525 and 550°C, indicates demagnetization of magnetite, as is further indicated by its low coercivity. The high coercivity component is probably related to a slight misalignment when applying the cross-component IRM, because of the small size of the HIP1 sample (Fig. 4c). In general, the high susceptibility, IRM acquisition curves and three-component

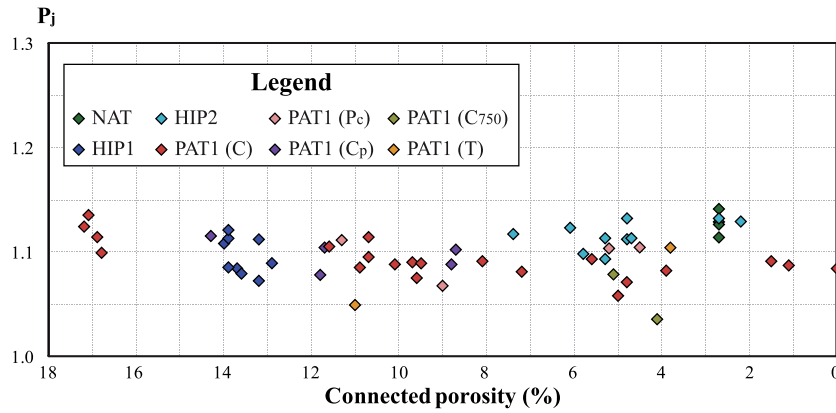


**Figure 5.** Low-field anisotropy of magnetic susceptibility (LF-AMS), expressed as  $P_j$  (Jelinek 1981), as a function of porosity of synthetic metapelites, colour-coded according to compaction history (Table 1). Natural Maplewood Shale (NAT) samples are included for comparison purposes.

demagnetization, and FORC behaviour are compatible with iron-sulphide as main magnetic phase and magnetite as minor phase. There is little evidence for the presence of high-coercivity phases, such as hematite and goethite.

Taking both synthesized and natural Maplewood Shale sample groups together, expressed as  $P_j$ , low-field AMS values vary between 1.04 and 1.14, with an average value of 1.09, regardless of sample porosity (Fig. 5). The average  $P_j$  value for the larger sample groups HIP1 and PAT1 (C) is comparable with the bulk average  $P_j$ . With 1.11 and 1.12, respectively, the average  $P_j$  for lithostatically compacted HIP2 samples and naturally compacted NAT samples contrast with that of non-lithostatically compacted samples.

The degree of ferrimagnetic AMS ( $\Delta k_f$ ) of the synthetic Maplewood Shale based metapelites as measured by torque magnetometry ranges between 1 and 11  $\mu\text{SI}$  (Fig. 6a). A majority of samples exhibit  $\Delta k_f$  values below 5  $\mu\text{SI}$  (trend (1)) and show no correlation with porosity. Furthermore, sample groups that fall within trend (1) represent compaction by different stress regimes; lithostatic for HIP1, HIP2 and PAT1 ( $P_c$ ) and non-lithostatic for PAT1 (C-C<sub>750</sub>-C<sub>p</sub>-T). Natural Maplewood Shale (NAT) fits trend 1 as well with  $\Delta k_f$  values below 2  $\mu\text{SI}$ . Only HIP2 samples and one PAT1 (T) sample have higher ferrimagnetic AMS. Because of a lack of data, no correlation between porosity and HIP2  $\Delta k_f$  could be established.  $\Delta k_f$  plotted against bulk magnetic susceptibility ( $K_m$ ) reveals a linear correlation with a coefficient of determination ( $R^2$ ) of 0.34 for the data points that belong to the synthetic samples in trend (1) of Fig. 6(a). Extrapolated to higher values for  $K_m$ , the best-fit linear curve approaches the HIP2 samples within 2.4  $\mu\text{SI}$ .

Overall, the degree of paramagnetic AMS ( $\Delta k_p$ ) is systematically larger than the ferrimagnetic AMS, ranging from nearly 12 to 17  $\mu\text{SI}$  at high porosity to 17 to 27  $\mu\text{SI}$  below 6 per cent porosity (Fig. 7a). A majority of data points, representing samples groups HIP1, HIP2 and PAT1 (C-P<sub>c</sub>-T), form a positive linear trend [trend (2) with  $R^2 = 0.53$ ] of increasing  $\Delta k_p$  with compaction. The inverse linear correlation of trend (2) is significant at 99.9 per cent confidence, using  $n = 16$  and correlation coefficient =  $-0.725$ . Both PAT1 (C<sub>750</sub>) and PAT1 (C<sub>p</sub>)  $\Delta k_p$  values plot systematically above trend (2). The natural Maplewood Shale (NAT) samples, plot within 3  $\mu\text{SI}$  of the best-fit curve for trend (2).

Considering only the synthetic metapelites and excluding three outliers, the minimum principal axis ( $k_3$ ) of the paramagnetic susceptibility shows a gradual, but non-linear, inclination steepening with compaction [trend (3) in Fig. 7b]. Trend (3) encompasses at least one sample from all sample groups, including four out of five

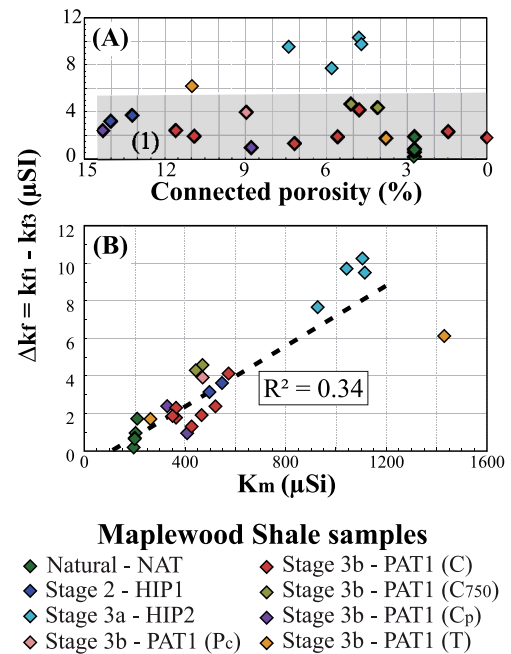


**Figure 6.** Data derived from the ferrimagnetic signal of the high-field anisotropy of magnetic susceptibility ( $\Delta k_p$ ) of natural Maplewood Shale and the experimentally compacted synthetic metapelites derived thereof. Samples are colour-coded according to compaction history (Table 1). Data on natural Maplewood Shale is added for comparison purposes. Values in parentheses are labels for trend lines. (a)  $\Delta k_f$  as a function of porosity. (b)  $\Delta k_f$  as a function of bulk magnetic susceptibility ( $K_m$ ). The best-fit linear curve in b is, except for NAT samples, derived from the samples of trend (1) in a.

of the naturally compacted NAT samples. Using  $n = 20$  and correlation coefficient =  $-0.359$ , even an inverse linear correlation for porosity and paramagnetic  $k_3$  inclination [trend (3)] was found to have significance until a significance level of 0.12, which relates to 88 per cent confidence. The other principal axes  $k_1$  and  $k_2$  remain shallow ( $<25^\circ$  inclination), regardless of porosity and compaction history. In an equal-area lower hemisphere stereographic projection, paramagnetic  $k_3$  of both the natural Maplewood Shale and the synthetic metapelites is centred, without preferred declination, around  $90^\circ$  dip, whereas  $k_1$  and  $k_2$  plot at low dip with scattered declination (Fig. 7c).

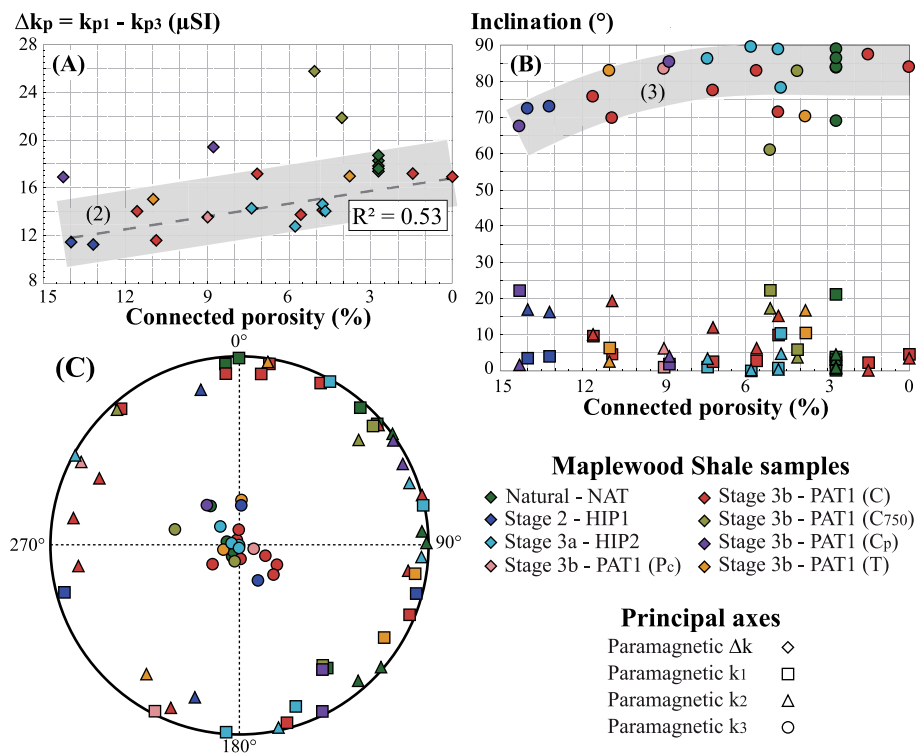


**Figure 7.** Data derived from the paramagnetic signal of the high-field anisotropy of magnetic susceptibility ( $\Delta k_p$ ) of illite shale powder that was experimentally compacted into synthetic metapelites. Samples are colour-coded according to compaction history (Table 1). Data on natural Maplewood Shale is added for comparison purposes. Values in parentheses are labels for trend lines. (a)  $\Delta k_p$  as a function of porosity. (b) Inclination data for the paramagnetic principal susceptibility axes as a function of porosity. (c) Equal area lower hemisphere projection for the directions of the paramagnetic principal susceptibility axes.

#### 4 DISCUSSION AND CONCLUSIONS

During sample preparation and experimental chemical compaction, bulk magnetic susceptibility of illite shale powder is repeatedly altered, reflecting primarily changes of the ferrimagnetic minerals (Table 1; Figs 2 and 3). Although not observed in Maplewood Shale fragments (NAT), in the crushed state [NAT (Pwd)] magnetite/maghemite is the principal remanence-carrying mineral (Fig. 3). The Maplewood Shale fragments (NAT) show negligible IRM acquisition, which is below the detection level of the VSM, and has considerably lower magnetic susceptibility (Table 1). Although attributed to inadvertent admixing of concretions or iron-oxide-bearing veins, the addition of magnetite/maghemite to Maplewood Shale powder [NAT (Pwd)] provided unique opportunities to monitor the behaviour of remanence-carrying minerals during experimental chemical compaction of illite shale powder. Magnetite/maghemite particles are heterogeneously distributed among the powder batches, as evidenced by the considerably varying bulk susceptibility of NAT (Pwd; Table 1). Contamination during the crushing procedure from an external source is excluded on grounds that powder of similarly treated Silver Hill shale has lower values for  $K_m$  (Bruijn 2012).

Rochette (1987) showed that marked changes in magnetic susceptibility in metapelites, typically correspond to changes in ferrimagnetic mineral content. He could couple observations of graded magnetic susceptibility in black shales of the Swiss Alps to demonstrate the breakdown reactions of magnetite and pyrite. Reduced susceptibility in our synthesized metapelites is attributed to the temperature and oxygen fugacity sensitive magnetite/maghemite breakdown reaction into pyrrhotite and pyrite, followed by the tem-

perature and sulphur fugacity sensitive breakdown reaction of pyrite into pyrrhotite (Crerar *et al.* 1978; Barker & Parks 1986).

The IRM acquisition curves for HIP1, HIP2 and PAT1 (C) samples, the two FORC distribution types with related IRM thermal demagnetization curves demonstrate unequivocally the existence of high-coercivity iron-sulphides such as pyrrhotite after compaction stage 2. Although a switch from multidomain to single-domain magnetite/maghemite because of grain size reduction can potentially reduce magnetic susceptibility and change AMS, it does not explain the IRM thermal demagnetization curves found in HIP1, HIP2 and PAT1 (C) samples and therefore seems an unlikely explanation for the observed magnetic susceptibility behaviour.

The similarity between natural observations by Rochette (1987) and our findings suggests that chemical conditions during compaction stages 2 and 3a compare to natural systems in which reducing conditions prevail, such as during regional metamorphism in the presence of graphite-buffered fluids (Ferry 1981; Mohr & Newton 1983; Hall 1986), and in mature claystones formed during rapid burial of organic matter (e.g. Aubourg & Pozzi 2010; Abdelmalak *et al.* 2012). Comparable susceptibility values for PAT1 and HIP1 samples (Table 1) suggests that the redox breakdown reactions completed during compaction stage 2. Higher susceptibility for HIP2 samples is attributed to higher initial magnetite/maghemite content, which resulted in a higher concentration of ferrimagnetic iron-sulphides after compaction stage 3a.

The ferrimagnetic AMS of synthetic metapelite sample groups is unaffected by compaction as  $\Delta k_f$  remains constant at a relative low value during compaction from 15 per cent to nearly 0 per cent porosity (Fig. 6a). As a similar behaviour was recorded for the low-field AMS, we conclude that besides bulk magnetic susceptibility also low-field AMS is controlled by the ferrimagnetic mineralogy

(Fig. 5). The apparent higher  $\Delta k_f$  for HIP2 samples (Fig. 6a) is rather a consequence of systematically higher bulk magnetic susceptibility than of enhanced preferred magnetocrystalline orientation for iron-sulphides, as indicated by the good agreement of HIP2 samples to the best-fit linear line in the  $K_m - \Delta k_f$  diagram (Fig. 6b). Similarly, natural Maplewood Shale (NAT) has relatively low  $\Delta k_f$  values primarily because of its low ferrimagnetic content, as is evident from its low bulk magnetic susceptibility (Table 1) and lack of notable hysteresis. The low-field AMS values reported for NAT samples are also explained by their low ferrimagnetic content and the greater contribution of aligned paramagnetic minerals to the AMS signal.

In this study, an inverse linear correlation between paramagnetic AMS and porosity was found [Fig. 7a trend (2)]. Orientation data of the paramagnetic susceptibility ellipsoid indicate that as porosity reduces, the short ( $k_3$ ) axis rotates towards steeper inclination without alignment of its declination, whereas the inclination of the intermediate ( $k_2$ ) and long ( $k_1$ ) axes becomes slightly shallower with scattered declination (Figs 7b and c). The described rotation of the paramagnetic susceptibility ellipsoid conforms to the development of a diagenetic foliation in pelites, as seen by the orientation of paramagnetic  $k_1$ ,  $k_2$  and  $k_3$  of NAT samples.

$\Delta k_p$  values for PAT1 (C-P<sub>c</sub>-T) samples plot within trend (2) of Fig. 7(a), which also includes HIP1 and HIP2 samples. This behavior is explained by enhanced illite crystallinity, which eventually leads to transformation of illite into phengite (Bruijn 2012). Compared with illite, mica minerals have higher crystallinity and single crystal AMS (Hrouda 1993). As such, not only porosity but also paramagnetic AMS are first-order measures of the progress of illite to phengite transformation. Higher  $\Delta k_p$  for PAT1 (C<sub>750</sub>) metapelites is explained by enhanced anisotropic biotite formation, which is not accompanied by pore closure (Bruijn 2012).

Application of pore pressure (Argon gas) in compaction stage 3b tests enhanced  $\Delta k_p$  for PAT1 (C<sub>p</sub>) samples compared with trend (2) (Fig. 7a). SEM BSE micrographs of PAT1 (C<sub>p</sub>) samples in Bruijn (2012) provide evidence for delayed chemical compaction, but enhanced detrital mica alignment in comparison with PAT1 (C) samples of comparable porosity. In addition, in one imaged PAT1 (C) sample, illite seems better preserved in pressure shadows of detrital quartz grains than in the phyllosilicate-rich matrix (Bruijn 2012). The rate of illite transformation and consequently chemical compaction can therefore be considered pore pressure dependent, with higher pore pressure restricting dissolution, solution transfer and precipitation reactions that make up phengite formation, as was observed in smectite illitization experiments by Whitney (1990). In addition, the combination of higher activation enthalpy for illite dehydration and reduced illite water expulsion rates in the presence of vapour pressure (Mikhail & Guindy 1971) is ultimately unfavourable for phengite formation. Strain in the stage 3b axial compression experiments with lower effective pressure (PAT1 (C<sub>p</sub>)) is therefore relatively more accommodated by mechanical grain rotation and microfolding than in standard axial compression experiments at 300 MPa confining pressure [PAT1 (C)]. The elevated  $\Delta k_p$  values for PAT1 (C<sub>p</sub>) samples (Fig. 7a) quantitatively demonstrate that the anisotropy development during compaction is more substantial when pores are closed by detrital grain rotation than by illite transformation and cementation.

Grain rotation as the primary mechanism of paramagnetic AMS development can be excluded on two grounds. First, trend (2) in Fig. 7(a) incorporates  $\Delta k_p$  data points from samples that experienced different compaction history in terms of the applied stress field and the resulting flow types (i.e. confining pressure yielding contraction, confined torsion and axial compression resulting in

simple and pure shear, respectively). In the process of grain rotation, the rotation history of material lines depends on the flow type by which it accumulated (e.g. Passchier & Trouw 2005). Therefore, if increased  $\Delta k_p$  is primarily the result of grain rotation of the long axis of illite and mica grains (i.e. material lines), then different flow types should give rise to unique and distinguishable  $\Delta k_p$  development trends. Secondly, the domain of diagenesis in which grain rotation is most observed is mechanical compaction, which in clay-rich sediments occurs in the smectite stability PT field above 70–90°C, corresponding typically to the top ~2 km of the sedimentary column (e.g. Athy 1930; Rieke & Chilingarian 1974; Hower *et al.* 1976; Aplin *et al.* 2003; Day-Stirrat *et al.* 2010). Experimental simulations of mechanical compaction of clay-rich sediments have shown that below ~15 per cent porosity the process is exhausted (e.g. Vasseur *et al.* 1995; Nygård *et al.* 2004; Mondol *et al.* 2007; Fawad *et al.* 2010). The non-linear strengthening of clays during mechanical compaction is the consequence of rapidly increasing resistance to mineral rotation and alignment. Chemical compaction in illite shale by mineral transformation and dissolution/precipitation processes is required to lower porosity below ~15 per cent. From the distinctly different paramagnetic and ferrimagnetic AMS development it is inferred that remanence-bearing minerals behave independently from illite and phengite minerals during chemical compaction below 15 per cent porosity.

As the AMS values of naturally compacted Maplewood Shale plot within the trend set out by the synthetic metapelites, there is good indication that comparable processes occurred in nature and the experimental simulations of illite mud diagenesis and metamorphism. The experiments of Bruijn (2012) bear direct relevance to natural systems where diagenesis grades into low-grade metamorphism and the illite transformation to phengite is activated. These systems can be found in collisional settings where (1) continental margin assemblages are subducted beneath another continent; or (2) sedimentary strata is scraped off the subducting oceanic plate and rotated, shortened and imbricated to form an accretionary prism on the margin of the overriding continental plate; or in c) extensional settings where relatively high heat flow resulted in steep geothermal gradients in the earliest basin infill (Merriman & Frey 1999).

In contrast with conclusions from mechanical compaction studies (Blow & Hamilton 1978; Anson & Kodama 1987; Deamer & Kodama 1990; Sun & Kodama 1992) theoretical work (Arason & Levi 1990a) and observation from nature (e.g. Arason & Levi 1990b), this study clearly demonstrates a decoupling between remanence-bearing minerals and paramagnetic phyllosilicates during chemical compaction of illite shale powder, regardless of the orientation of the stress field. Caution is therefore required when interpreting remanence magnetization or low-field AMS data of both deformed and undeformed chemically compacted mudstones and shales in the context of texture, compaction, strain, or physical properties as the ferrimagnetic and paramagnetic minerals may have developed independently during the later stages of mud diagenesis or early stages of pelite metamorphism.

## ACKNOWLEDGMENTS

We thank S. Misra for running the HIP apparatus during compaction stage 2 and 3a experiments, R. Hofmann for technical support and L. Lanzi for performing thermal demagnetization of IRM analysis on two of our samples. Two anonymous reviewers and editor J. Renner are acknowledged for their extensive commentary. This research was funded by SNF projects 200020–132772 and 200021–116153.

## REFERENCES

- Abdelmalak, M.M., Aubourg, C., Geoffroy, L. & Laggoun-Défarge, F., 2012. A new oil-window indicator? The magnetic assemblage of claystones from the Baffin Bay volcanic margin (Greenland), *AAPG Bull.*, **92**(2), 205–215.
- Anson, G.L. & Kodama, K.P., 1987. Compaction-induced inclination shallowing of the post-depositional remanent magnetization in a synthetic sediment, *Geophys. J. R. astr. Soc.*, **88**(3), 673–692.
- Aplin, A.C., Matenaar, I.F. & Van der Pluijm, B.A., 2003. Influence of mechanical compaction and chemical diagenesis on the microfabric and fluid flow properties of Gulf of Mexico mudstones, *J. Geochem. Explor.*, **78–79**, 449–451.
- Arason, P. & Levi, S., 1990a. Models of inclination shallowing during sediment compaction, *J. geophys. Res.*, **95**(B4), 4481–4499.
- Arason, P. & Levi, S., 1990b. Compaction and inclination shallowing in deep-sea sediments from the Pacific Ocean, *J. geophys. Res.*, **95**(B4), 4501–4510.
- Athy, L.F., 1930. Density, porosity, and compaction of sedimentary rocks, *AAPG Bull.*, **14**(1), 25–35.
- Aubourg, C. & Pozzi, J-P., 2010. Towards a new <250°C pyrrhotite-magnetite geothermometer for claystones, *Earth planet. Sci. Lett.*, **294**, 47–57.
- Barker, W.W. & Parks, T.C., 1986. The thermodynamic properties of pyrrhotite and pyrite: a re-evaluation, *Geochim. cosmochim. Acta.*, **50**(10), 2185–2194.
- Bergmüller, F., Barlocher, C., Geyer, B., Grieder, M., Heller, F. & Zweifel, P., 1994. A torque magnetometer for measurements of the high-field anisotropy of rocks and crystals, *Meas. Sci. Tech.*, **5**(12), 1466–1470.
- Bjørlykke, K., 1998. Clay mineral diagenesis in sedimentary basins—a key to the prediction of rock properties. Examples from the North Sea Basin, *Clay Miner.*, **33**, 15–34.
- Blow, R.A. & Hamilton, N., 1978. Effect of compaction on the acquisition of a detrital remanent magnetization in fine-grained sediments, *Geophys. J. R. astr. Soc.*, **52**(1), 13–23.
- Boles, J.R. & Franks, S.G., 1979. Clay diagenesis in Wilcox sandstones of southwest Texas: implications of smectite diagenesis on sandstone cementation, *J. Sedim. Petrol.*, **49**(1), 55–70.
- Brett, C.E., Goodman, W.M. & LoDuca, S.T., 1990. Sequences, cycles, and basin dynamics in the Silurian of the Appalachian Foreland Basin, *Sedim. Geol.*, **69**, 191–244, doi:10.1016/0037-0738(90)90051-T.
- Bruijn, R.H.C., 2012. Chemical compaction of illite shale: an experimental study, *PhD thesis*, ETH Zurich, Zurich.
- Crerar, D.A., Susak, N.J., Borcsik, M. & Schwartz, S., 1978. Solubility of the buffer assemblage pyrite + pyrrhotite + magnetite in NaCl solutions from 200 to 350°C, *Geochim. cosmochim. Acta.*, **42**(9), 1427–1437.
- Day-Stirrat, R.J., Milliken, K.L., Dutton, S.P., Loucks, R.G., Hillier, S., Aplin, A.C. & Schleicher, A.M., 2010. Open-system chemical behavior in deep Wilcox Group mudstones, Texas Gulf Coast, USA, *Mar. Petrol. Geol.*, **27**(9), 1804–1818.
- Deamer, G.A. & Kodama, K.P., 1990. Compaction-induced inclination shallowing in synthetic and natural clay-rich sediments, *J. geophys. Res.*, **95**(B4), 4511–4529.
- Dunlop, D.J. & Özdemir, Ö., 1997. *Rock Magnetism: Fundamentals and Frontiers*, pp. 596, Cambridge University Press, Cambridge.
- Fawad, M., Mondol, N.H., Jahren, J. & Bjørlykke, K., 2010. Microfabric and rock properties of experimentally compressed silt-clay mixtures, *Mar. Petrol. Geol.*, **27**, 1698–1712.
- Ferry, M.J., 1981. Petrology of graphitic sulfide-rich schists from south-central Maine: an example of desulfidation during prograde regional metamorphism, *Am. Mineral.*, **66**, 908–930.
- Friedman, G.M., 1987. Vertical movements of the crust: case histories from the northern Appalachian Basin, *Geology*, **15**(12), 1130–1133.
- Hall, A.J., 1986. Pyrite-pyrrhotite redox reactions in nature, *Mineral. Mag.*, **50**, 223–229.
- Harrison, R.J. & Feinberg, J.M., 2008. FORCinel: an improved algorithm for calculating first-order reversal curve distributions using locally weighted regression smoothing, *Geochem. Geophys. Geosyst.*, **9**, doi:10.1029/2008GC001987.
- Hower, J., Eslinger, E.V., Hower, M.E. & Perry, E.A., 1976. Mechanism of burial metamorphism of argillaceous sediment: 1. Mineralogical and chemical evidence, *Bull. geol. Soc. Am.*, **87**(5), 725–737.
- Hrouda, F., 1993. Theoretical models of magnetic anisotropy to strain relationship revisited, *Phys. Earth planet. Inter.*, **77**(3–4), 237–249.
- Jackson, M.J., Banerjee, S.K., Marvin, J.A., Lu, R. & Gruber, W., 1991. Detrital remanence, inclination errors, and anhysteretic remanence anisotropy: quantitative model and experimental results, *Geophys. J. Int.*, **104**(1), 95–103.
- Jelínek, V., 1981. Characterization of the magnetic fabric of rocks, *Tectonophysics*, **79**(3–4), T63–T67.
- Kaszuba, J.P., Janecky, D.R. & Snow, M.G., 2005. Experimental evaluation of mixed fluid reactions between supercritical carbon dioxide and NaCl brine: relevance to the integrity of a geologic carbon repository, *Chem. Geol.*, **217**(3), 277–293.
- Katari, K. & Tauxe, L., 2000. Effects of pH and salinity on the intensity of magnetization in redeposited sediments, *Earth planet. Sci. Lett.*, **181**(4), 489–496.
- Land, L.S., Mack, L.E., Milliken, K.L. & Lynch, F.L., 1997. Burial diagenesis of argillaceous sediment, south Texas Gulf of Mexico sedimentary basin: a reexamination, *Bull. geol. Soc. Am.*, **109**(1), 2–15.
- Lowrie, W., 1990. Identification of ferromagnetic minerals in a rock by coercivity and unblocking temperature properties, *Geoph. Res. Lett.*, **17**(2), 159–162.
- Lu, R., Banerjee, S.K. & Marvin, J., 1990. Effects of clay mineralogy and the electrical conductivity of water on the acquisition of depositional remanent magnetization in sediments, *J. geophys. Res.*, **95**, 4531–4538.
- Martín-Hernández, F. & Hirt, A.M., 2001. Separation of ferrimagnetic and paramagnetic anisotropies using a high-field torsion magnetometer, *Tectonophysics*, **337**(3–4), 209–221.
- Merriman, R.J. & Peacor, D.R., 1999. Very low-grade metapelites: mineralogy, microfabrics and measuring reaction progress, in *Low-Grade Metamorphism*, pp. 10–60, eds Frey, M. & Robinson, D., Blackwell Science Ltd., Oxford.
- Merriman, R.J. & Frey, M., 1999. Patterns of very low-grade metamorphism in metapelitic rocks, in *Low-grade metamorphism*, pp. 61–107, eds Frey, M. & Robinson, D., Blackwell Science Ltd., Oxford.
- Mikhail, R.Sh. & Guindy, N.M., 1971. Rates of low-temperature dehydration of montmorillonite and illite, *J. Appl. Chem. Biotechnol.*, **21**(4), 113–116.
- Mohr, D.W. & Newton, R.C., 1983. Kyanite-staurolite metamorphism in sulfidic schists of the Anakeeste Formation, Great smoky Mountains, North Carolina, *Am. J. Sci.*, **283**, 97–134.
- Mondol, N.H., Bjørlykke, K., Jahren, J. & Høeg, K., 2007. Experimental mechanical compaction of clay mineral aggregates—changes in physical properties of mudstones during burial, *Mar. Petrol. Geol.*, **24**(5), 289–311.
- Nygård, R., Gutierrez, M., Gautam, R. & Høeg, K., 2004. Compaction behavior of argillaceous sediments as function of diagenesis, *Mar. Petrol. Geol.*, **21**(3), 349–362.
- Passchier, C.W. & Trouw, R.A.J., 2005. *Microtectonics*, 2nd edn, pp. 366, Springer Verlag, Berlin, Heidelberg.
- Paterson, M.S., 1990. Rock deformation experimentation, in *The Brittle-Ductile Transition in Rocks. The Heard Volume*, Geophys. Monograph Vol. 56, pp. 187–194, ed. Duba, A.G., AGU, Washington, DC.
- Paterson, M.S. & Olgaard, D.L., 2000. Rock deformation tests to large shear strains in torsion, *J. Struct. Geol.*, **22**(9), 1341–1358, doi:10.1016/S0191-8141(00)00042-0.
- Peltonen, C., Marcussen, Ø., Bjørlykke, K. & Jahren, J., 2009. Clay mineral diagenesis and quartz cementation in mudstones: the effects of smectite to illite reaction on rock properties, *Mar. Petrol. Geol.*, **26**, 887–898.
- Pike, C.R., Roberts, A.P. & Verosub, K.L., 1999. Characterizing interactions in fine magnetic particle systems using first order reversal curves, *J. Appl. Phys.*, **85**(9), 6660–6667.
- Rieke, H.H. III & Chilingarian, G.V., 1974. *Compaction of Argillaceous Sediments*, p. 424, Elsevier Sci. Pub. Co., Amsterdam.

- Roberts, A.P., Chang, L., Rowan, C.J., Horng, C.-S. & Florindo, F., 2011. Magnetic properties of sedimentary greigite ( $\text{Fe}_3\text{S}_4$ ): an update, *Rev. Geophys.*, **49**(doi:10.1029/2010RG000336).
- Roberts, A.P., Liu, Q., Rowan, C.J., Chang, L., Carvalho, C., Torrent, J. & Horng, C.-S., 2006. Characterization of hematite ( $\alpha\text{-Fe}_2\text{O}_3$ ), goethite ( $\alpha\text{-FeOOH}$ ), greigite ( $\text{Fe}_3\text{S}_4$ ), and pyrrhotite ( $\text{Fe}_7\text{S}_8$ ) using first-order reversal curve diagrams, *J. geophys. Res.*, **111**, B12S35, doi:10.1029/2006JB004715.
- Roberts, A.P., Pike, C.R. & Verosub, K.L., 2000. First-order reversal curve diagrams: a new tool for characterizing the magnetic properties of natural samples, *J. geophys. Res.*, **105**(B12), 28 461–28 475.
- Rochette, P., 1987. Metamorphic control of the magnetic mineralogy of black shales in the Swiss Alps: toward the use of “magnetic isogrades”, *Earth planet. Sci. Lett.*, **84**(4), 446–456.
- Rogers, W.B., Isachsen, Y.W., Mock, T.D. & Nyahay, R.E., 1990. *New York State Geological Highway Map*, New York State Museum/Geological Survey, Albany, New York.
- Saffer, D.M. & Marone, C., 2003. Comparison of smectite- and illite-rich gouge frictional properties: application to the updip limit of the seismogenic zone along subduction megathrusts, *Earth planet. Sci. Lett.*, **215**(1), 219–235.
- Schneider, J., Flemings, P.B., Day-Stirrat, R.J. & Germaine, J.T., 2011. Insights into pore-scale controls on mudstone permeability through resedimentation experiments, *Geology*, **39**(11), 1011–1014.
- Sun, W.W. & Kodama, K.P., 1992. Magnetic anisotropy, scanning electron microscopy, and X-ray pole figure goniometry study of inclination shallowing in a compacting clay-rich sediment, *J. geophys. Res.*, **97**(B13), 19 599–19 615.
- Till, J.L., Jackson, M.J. & Moskowitz, B.M., 2010. Remanence stability and magnetic fabric development in synthetic shear zones deformed at 500°C, *Geochem. Geophys. Geosys.*, **11**, Q12Z21, doi:10.1029/2010GC003320.
- Towe, K.M., 1962. Clay mineral diagenesis as a possible source of silica cement in sedimentary rocks, *J. Sedim. Petrol.*, **32**(1), 26–28.
- Van de Kamp, P.C., 2008. Smectite-illite-muscovite transformations, quartz dissolution, and silica release in shales, *Clays and Clay Minerals*, **56**(1), 66–81.
- Vasseur, G., Djeran-Maigre, I., Grunberger, D., Rousset, G., Tessier, D. & Velde, B., 1995. Evolution of structural and physical parameters of clays during experimental compaction, *Mar. Petrol. Geol.*, **12**(8), 941–954.
- Voltolini, M., Wenk, H.-R., Mondol, N.H., Bjørlykke, K. & Jähren, J., 2009. Anisotropy of experimentally compressed kaolinite-illite-quartz mixtures, *Geophysics*, **74**(1), D13–D22.
- Whitney, G., 1990. Role of water in the smectite-to-illite reaction, *Clays Clay Miner.*, **38**(4), 343–350.